Structural systematics and conformational analyses of a 3 × 3 isomer grid of fluoro-N-(pyridyl)benz-amides: physicochemical correlations, poly-morphism and isomorphous relationships

Pavle Mocilac, Katie Donnelly and John F. Gallagher*

Targeted Therapeutics and Theranostics (T3) Programme, School of Chemical Sciences, Dublin City University, Dublin 9, Ireland

Correspondence e-mail: john.gallagher@dcu.ie

An isomer grid of nine fluoro-N-(pyridyl)benzamides (**Fxx**) (**x** = *para*-/*meta*-/*ortho*-) has been examined to correlate structural relationships between the experimental crystal structure and *ab initio* calculations, based on the effect of fluorine (**Fx**) and pyridine N-atom (**x**) substitution patterns on molecular conformation. Eight isomers form N—H$\cdots$N hydrogen bonds, and only one (**Fom**) aggregates *via* intermolecular N—H$\cdots$O$=$C interactions exclusively. The **Fpm** and **Fom** isomers both crystallize as two polymorphs with **Fpm_O** (N—H$\cdots$O$=$C chains, **P-syn**) and **Fpm_N** (N—H$\cdots$N chains, **P-anti**) both in $P2_1/n$ ($Z' = 1$) differing by their *meta*-N atom locations (**P-syn**, **P-anti**; $N_{pyridine}$ referenced to N—H), whereas the disordered **Fom_O** is mostly **P-syn** ($Z' = 6$) compared with **Fom_F** (**P-anti**) ($Z' = 1$). In the **Fxo** triad twisted dimers form cyclic $R_2^2(8)$ rings *via* N—H$\cdots$N interactions. Computational modelling and conformational preferences of the isomer grid demonstrate that the solid-state conformations generally conform with the most stable calculated conformations except for the **Fxm** triad, while calculations of the **Fox** triad predict the intramolecular N—H$\cdots$F interaction established by spectroscopic and crystallographic data. Comparisons of **Fxx** with related isomer grids reveal a high degree of similarity in solid-state aggregation and physicochemical properties, while correlation of the melting point behaviour indicates the significance of the substituent position on melting point behaviour rather than the nature of the substituent.

1. Introduction

Fluorine structural chemistry continues to flourish in crystal engineering and structural studies, as well as in the systematic design of new functional materials (Berger *et al.*, 2011; Chopra & Row, 2011; Metrangolo *et al.*, 2011; Ren *et al.*, 2011). Isomer grids containing fluorine or other halogen atoms have formed part or all of a variety of structural studies reported in the past decade (Luthe *et al.*, 2007; Gelbrich *et al.*, 2007; Wardell *et al.*, 2007, 2008; Chopra & Row, 2008; Mocilac *et al.*, 2011). The importance of such studies is to lay a foundation whereupon grids can be expanded and from which physicochemical correlations and structure–activity relationships can be derived and evaluated. Our interest in fluorine chemistry arises from our on-going studies of $n \times m$ isomer grids ($n, m \geq$ 3), *e.g.* **NxxF** (Mocilac *et al.*, 2011) so as to examine relationships of interchanging H/F/CH$_3$ atoms/groups in a structural systematic fashion about (hetero)aromatic rings, as well as probing organic F atoms in unusual environments and fluorine participating in atypical interactions.

Table 1
Selected crystallographic data for the **Fxx** isomers.

Fxx = $C_{12}H_9N_2OF$, M_r = 216.21, $F(000)$ = 448, T = 294 K. R-factors defined by $R[F^2 > 2\sigma(F^2)]$, $wR(F^2)$; NV = No. of parameters.

Structure	Space group	Z/Z'	Cell parameters (Å, °), V (Å³)	θ_{max} (°), R_{int}, $(\sin\theta/\lambda)_{max}$ (Å^{-1})	R, wR, S, N_{ref}, NV
Fpp†	$P2_1/c$	4/1	5.6777 (1), 11.4769 (2), 15.5289 (3), 90, 95.974 (2), 90, 1006.40 (3)	27.8, 0.013, 0.656	0.034, 0.090, 1.04, 2216, 150
Fmp†	$P2_1/c$	4/1	5.7961 (1), 11.3050 (2), 15.2384 (2), 90, 94.238 (1), 90, 995.76 (3)	27.8, 0.012, 0.656	0.034, 0.092, 1.05, 2202, 150
Fop†	$P2_1/c$	4/1	6.0388 (1), 11.2502 (2), 14.9265 (3), 90, 95.310 (2), 90, 1009.72 (3)	27.9, 0.016, 0.658	0.037, 0.103, 1.02, 2256, 150
Fpm_O	$P2_1/n$	4/1	13.9411 (3), 5.2040 (1), 15.0752 (3), 90, 114.812 (3), 90, 992.74 (3)	29.6, 0.012, 0.695	0.042, 0.114, 1.03, 2624, 150
Fpm_N	$P2_1/n$	4/1	3.9077 (2), 24.2444 (12), 10.7012 (5), 90, 95.181 (5), 90, 1009.69 (9)	27.4, 0.049, 0.647	0.053, 0.120, 0.96, 2162, 149
Fmm	$Pca2_1$	4/1	11.3020 (3), 11.8371 (3), 7.6218 (2), 90, 90, 90, 1019.67 (5)	27.8, 0.021, 0.656	0.033, 0.084, 1.02, 1239, 149
Fom_O	$P2_1$	12/6	16.2051 (4), 5.2239 (1), 35.8162 (9), 90, 98.405 (3), 90, 2999.41 (12)	58.3, 0.026, 0.552	0.059, 0.176, 1.06, 5835, 1315
Fom_F	$P2_1/n$	4/1	5.4788 (2), 8.8223 (4), 20.4414 (7), 90, 92.150 (4), 90, 987.35 (7)	27.8, 0.027, 0.655	0.044, 0.122, 1.05, 2178, 149
Fpo	$Pbcn$	8/1	24.3381 (4), 10.7183 (4), 10.8791 (2), 90, 90, 90, 2100.58 (6)	27.1, 0.024, 0.640	0.042, 0.113, 1.04, 2254, 150
Fmo	$P\bar{1}$	4/2	10.4219 (4), 10.7183 (4), 11.0188 (3), 102.286 (3), 97.356 (3), 117.074 (4), 1034.48 (6)	27.9, 0.016, 0.659	0.046, 0.124, 1.03, 4555, 298
Foo	$P\bar{1}$	4/2	9.7560 (4), 10.7699 (5), 11.9694 (2), 64.412 (4), 68.453 (4), 86.091 (4), 1048.88 (7)	29.5, 0.012, 0.692	0.044, 0.114, 1.04, 5437, 298

† **Fxp** = LOCREB, LOCLEV, LOCRAX at 150 K (Donnelly *et al.*, 2008; Allen, 2002).

Isomorphous relationships have been noted in a series of benzamides where H/F atoms have been swopped in an aromatic ring (Donnelly *et al.*, 2008). Given the isosteric relationship that fluorine has with the H atom and the ability of fluorine to participate in weak interactions (Berger *et al.*, 2011), there is ample evidence that a wealth of interesting structural motifs involving 'organic fluorine' will be revealed in systematic studies ($n \times m$ isomer grids). Using this approach, we have conducted high-level *ab initio* geometry optimizations and conformational analyses of isomer grids to appraise differences (where they arise) between solid-state conformations and global minima (GM) derived from calculations (Mocilac *et al.*, 2010, 2011; Mocilac & Gallagher, 2011).

Scheme 1
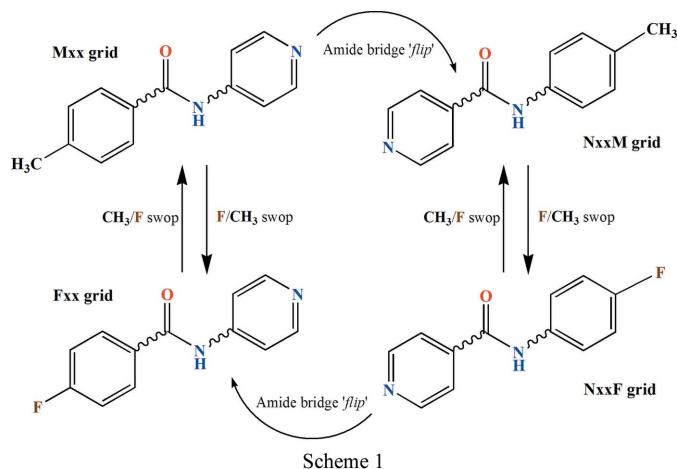
We herein report on the analysis of a 3×3 isomer grid of nine fluoro-*N*-(pyridyl)benzamides (**Fxx**) ($C_{12}H_9N_2OF$) including two pairs of polymorphs (for **Fpm** and **Fom**), where **Fx** and **x** represent the fluorobenzoyl and aminopyridine components, respectively, and determining the substitution pattern on either C_6 or C_5N aromatic ring (Scheme 1). Our comprehensive study integrates crystal structure analyses, computational chemistry and conformational analysis for the

Fxx isomer grid together with an investigation of physico-chemical trends using ^{1}H NMR and IR spectroscopy and melting point analysis. Detailed comparisons are made with three related 3×3 isomer grids, *i.e.* **Mxx**, **NxxM** and **NxxF**.

2. Experimental

2.1. Materials and equipment

The vendors, analytical and spectroscopic equipment together with spectroscopic and computational methods used in this research are as reported previously (Mocilac *et al.*, 2010, 2011; Mocilac & Gallagher, 2011).

2.2. General description of the Fxx synthesis

All nine **Fxx** isomers were synthesized using standard nucleophilic acyl substitution reactions (Schötten–Baumann reaction) between the 4-/3-/2-aminopyridines and 4-/3-/2-fluorobenzoyl chlorides at 294 K. The general procedure is as described for the **Fxp** triad of compounds (Donnelly *et al.*, 2008): an alternative route is reported by Lu *et al.* (2003). The **Fxm** isomers were prepared by the condensation reaction of 3-aminopyridine (3-AP) with 4-/3-/2-fluorobenzoyl chlorides in CH_2Cl_2 in the presence of 1 equiv of triethylamine (Et_3N). Crystalline products were obtained after purification using column chromatography.

A different procedure was used for the **Fxo** triad, as the 2-aminopyridine (2-AP) exhibits increased reactivity due to the *ortho* N atom and readily undergoes a dibenzoylation reaction giving the (2:1) imides (**Fxod**) as a side-reaction (Gallagher *et al.*, 2009*a,b*) and thus lowering the overall **Fxo** yields. Therefore, synthesis of the **Fxo** triad was performed at lower temperatures (263 K) with no catalytic base and an excess of 2-AP with pyridine as a solvent. The pyridine forms a strong N—H···N hydrogen bond with the amide H atom and presumably protecting it from a second benzoylation reaction. The resulting crystalline **Fxo** compounds were separated from

Table 2
Salient interplanar angle and intermolecular packing details (Å,°).

Structure†	C$_6$/C$_5$N	C$_6$/amide‡	C$_5$N/amide‡	N···N/O	Packing§
Fpp	52.14 (4)	33.51 (5)	18.93 (6)	3.0581 (15)	C(6) chains
Fmp	48.86 (4)	32.37 (5)	17.55 (6)	3.0786 (14)	C(6) chains
Fop	46.14 (4)	31.65 (5)	15.20 (7)	3.0587 (16)	C(6) chains
Fpm_O	1.02 (9)	31.25 (6)	30.32 (6)	3.0575 (13)	C(4) chains
Fpm_N	28.95 (8)	20.73 (9)	8.40 (9)	3.151 (3)	C(5) chains
Fmm	43.97 (6)	35.95 (7)	8.02 (9)	3.077 (3)	C(5) chains
Fom_F†	2.35 (10)	18.36 (8)	16.14 (8)	3.3321 (17)	C(4) chains
Fpo	44.41 (5)	39.56 (5)	6.19 (5)	3.0608 (18)	$R_2^2(8)$ rings
Fmo A	65.30 (6)	49.48 (7)	16.47 (7)	3.0721 (17)	$R_2^2(8)$ rings
B	47.92 (6)	43.00 (8)	6.39 (14)	3.0502 (18)	
Foo A	66.31 (5)	69.18 (6)	4.61 (9)	3.0460 (14)	$R_2^2(8)$ rings
B	52.02 (5)	38.12 (6)	15.71 (3)	3.0408 (15)	

† The **Fom_O** disorder ($Z' = 6$) is discussed in §3.3.3 and the supplementary material.   ‡ Amide plane calculated as a five-atom plane as [C−(C═O)N−C].   § Primary packing descriptors using graph-set notation (Etter, 1990); chains are one-dimensional (*zigzag*); $R_2^2(8)$ rings, cyclic as (N−H···N)$_2$.

Table 3
Melting points for **Mxx**, **NxxM**, **NxxF** and **Fxx** isomer grids.

Average melting-point range for all 36 isomers with highest melting point denoted by $^{\$}$, lowest by *. The N−H···N interactions are in bold italics and the N−H···O═C in italics: melting points for non-centrosymmetric space groups are underlined.

Mxx	Mp	Mm	Mo	No	Nm	Np	NxxM
p	*181$^{\$}$*	*106*	<u>*129*</u>	<u>*105*</u>	*148*	*162$^{\$}$*	**pM**
m	<u>*128*</u>	*91*	<u>*108*</u>	<u>*50**</u>	*114*	*142*	**mM**
o	<u>*105*</u>	*79**	<u>*116*</u>	<u>*65*</u>	*107*	<u>*125*</u>	**oM**
o	*120*	*77**	*85*	*107*	<u>*117*</u>	<u>*140$^{\$}$*</u>	**oF**
m	*150, 148*	<u>*151*</u>	*89*	*78**	<u>*122*</u>	<u>*132*</u>	**mF**
p	*187$^{\$}$*	<u>*186*</u>	*135*	*94*	*132*	<u>*135*</u>	**pF**
Fxx†	**Fp**	**Fm**	**Fo**	**No**	**Nm**	**Np**	**NxxF**

† Present study.

the corresponding **Fxod** imides by chromatography. Detailed descriptions of the synthetic and purification procedures are provided in the supplementary material[1] (§1).

2.3. Single-crystal growth and X-ray crystallography methods

Single crystals of the **Fxx** isomers including the three **Fxp** compounds (Donnelly *et al.*, 2008) were obtained by slow evaporation of solutions at 277 or 294 K and typically from ethyl acetate, while **Fmo** was grown from CDCl$_3$. The only **Fxx** isomer that proved difficult to crystallize as diffraction quality crystals was **Fom**: decent quality crystals were only obtained after a series of crystal growth experiments from mixtures of methanol and diethyl ether. All X-ray data were collected using Mo radiation on a Gemini S Ultra diffractometer at 294 K, with θ in the range 2–25° and 100% data coverage to 25° on θ (Oxford Diffraction, 2010), except for **Fom_O** (Cu radiation used). Data reduction procedures and absorption corrections are standard and comprehensive details have been published elsewhere (Oxford Diffraction, 2010). All structures

were solved using the *SHELXS*97 direct-methods program (Sheldrick, 2008) and refined by full-matrix least-squares calculations on F^2 with all non-H atoms having anisotropic displacement parameters using *SHELXL*97 (Sheldrick, 2008) and the *OSCAIL* software package (McArdle, 1995). H atoms were treated as riding atoms using the *SHELXL*97 defaults (at 294 K) except for the amide N−H (isotropic refinement). Selected crystallographic and structural information are provided in Tables 1, 2 and supplementary material (the amide as a five atom plane) with melting point data in Table 3. The disordered **Fom_O** structure was subject to extensive restraints, isotropic refinement and with the amide H treated as a riding atom. Molecular and hydrogen-bonding diagrams (Figs. 1–5) were generated using *Mercury* (Macrae *et al.*, 2008) and *PLATON* (Spek, 2009). All searches on the Cambridge Structural Database (CSD) were performed with the November 2010 release (Version 5.32+5 updates; Allen, 2002).

2.4. Computational methods

The computational methods and procedures reported herein are similar to previous research (Mocilac *et al.*, 2010, 2011; Mocilac & Gallagher, 2011) using *Gaussian*03/09 (Frisch *et al.*, 2010). The *ab initio* DFT (B3LYP) geometry optimizations (*gas phase*) were performed using the B3LYP/6–311++G** basis set; related analyses with/without the polarization/diffuse functions are provided in the supplementary material (§5). Solvated geometry optimizations and conformational analyses were performed in CH$_2$Cl$_2$ and H$_2$O (PCM-SMD solvation model, PCM-SMD = polarizable continuum model-solvation model density; Marenich *et al.*, 2009) specifically using the B3LYP/6-311++G** basis set. Additionally, high-
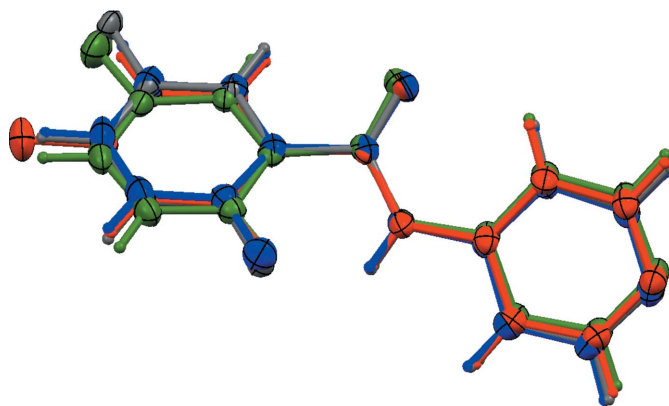
Figure 1
An overlay of the three isomorphous **Fxp** (red, green, blue) and **25_F$_2$** (grey) derivatives with displacement ellipsoids at the 30% probability level.

Pavle Mocilac *et al.* · Structural systematics and conformational analyses

Table 4
Torsion angles (°) of optimized **Fxx** isomers.

The angle C12—C11—C1═O1 (**F**-ring) is α; angle C1—N1—C21—C26 angle (**P**-ring) is β and O1—C1—N1—C21 angle (amide linkage) is δ. All geometries are based on B3LYP/6-311++G** optimization with the PCM-SMD solvation model.

	Optimized in *gas phase*			Optimized in CH_2Cl_2			Optimized in H_2O		
	α (°)	β (°)	δ (°)	α (°)	β (°)	δ (°)	α (°)	β (°)	δ (°)
Fpp	−24.45	−5.33	−3.10	−25.49	−6.72	−3.14	−26.21	−12.01	−3.10
Fmp	−24.95	−4.70	−2.85	−24.78	−4.47	−2.93	−24.43	−6.72	−3.40
Fop	−0.03	0.01	0.03	0.01	0.00	0.00	−0.01	0.00	0.00
Fpm	−24.27	−5.67	−2.51	−25.36	−7.76	−2.71	−25.52	−16.41	−2.10
Fmm	−24.62	−4.79	−2.29	−24.62	−5.38	−2.43	−23.91	−12.62	−1.64
Fom	0.01	0.00	−0.02	−0.05	0.00	0.00	−6.62	−4.48	−0.68
Fpo	−21.73	−3.44	−2.66	−25.54	−7.43	−2.10	−25.08	−6.11	−3.06
Fmo	−22.08	−2.96	−2.55	−24.27	−3.76	−2.17	−24.16	−5.63	−3.66
Foo	−0.01	0.00	0.00	−7.51	0.79	0.48	−7.65	−3.96	0.16

accuracy energy calculations including ΔG_{solv} were acquired using the CBS-QB3 compound method (Montgomery *et al.*, 1994), see supplementary material.

The conformational analysis of each **Fxx** structure was undertaken using PES scans (±180°) of the two key C12—C11—C1═O1 (α, **F**-ring) and C1—N1—C21—C26 (β, **P**-ring) dihedral angles both in *gas phase* and solvents. Each asymmetric (*meta-* or *ortho-*) fluorophenyl (**F**-ring) or pyridine (**P**-ring) ring can adopt, relative to the amide linker, two conformations (*syn* or *anti*; see Scheme 2), as denoted by *syn* (**F-syn, P-syn**) or *anti* (**F-anti, P-anti**). Rings with a *para*-phenyl F atom and/or *para*-pyridine N are not subject to this convention. The results provide PES diagrams highlighting conformation preferences (*syn/anti*) and with rotational barriers in kJ mol^{-1} (Table 4).

Scheme 2
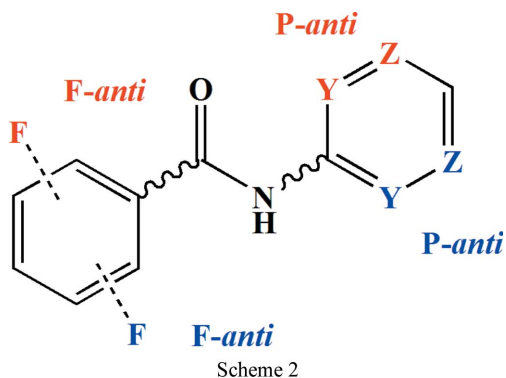
Computational analyses were performed to:

(i) investigate the overall changes in molecular geometry and conformation,

(ii) facilitate comparisons of the optimized structures and conformations with the solid-state structural results and

(iii) examine the influence of the solvation model (CH_2Cl_2, H_2O; PCM-SMD method) on the **Fxx** molecular geometry and conformations.

Our analyses appraise the **Fxx** *gas phase* and solvated conformational preferences with the solid-state geometries, as well as review trends with the **Mxx**, **NxxM** and **NxxF** isomer grids (Scheme 1).

3. Results and discussion

3.1. Comment on synthesis and general characteristics

The **Fxx** compounds (as expected for benzamides) are crystalline, colourless, odourless solids, readily soluble in most organic solvents, less soluble in cyclohexane and diethylether, but insoluble in water. The yields (supplementary material) were excellent for the **Fxp/Fxm** isomers, but lower for **Fxo** due to the competing reaction (§2.2) and strategies were employed to prevent a significant formation of **Fxod** imide side-products (Gallagher *et al.*, 2009*a,b*; Mocilac *et al.*, 2010). The compound purities, following standard purification and chromatography, were excellent as analysed by thin layer chromatography. In related benzamides (Mocilac *et al.*, 2010, 2011; Mocilac & Gallagher, 2011) we noted similar melting point trends with melting point ranges and median values dropping from the symmetrical **Fpp** to the less symmetrical isomers, with **Fmo** having the lowest melting point. The melting points of **Fop** and **Fom** are ∼ 50 K lower than the related isomers in the **Mxx**, **NxxM** and **NxxF** series (Table 3, §3.4).

3.2. Comment on spectroscopic data

All spectroscopic data, including ^1H, ^{13}C, ^{19}F NMR and IR spectra are presented in the supplementary material (§§2 and 3) and a high degree of modularity is present within the **P** and **F** rings (Mocilac *et al.*, 2010, 2011; Mocilac & Gallagher, 2011).

The amide proton (δ_{N-H}) resonance at *ca* 8.37 p.p.m. (CDCl$_3$) shifts to 10.62 p.p.m. (DMSO-d_6) for the six **Fxp/Fxm** isomers. However, the average δ_{N-H} for **Fxo** is *ca* 8.94 p.p.m. (CDCl$_3$), shifted to ∼ 10.85 p.p.m. in DMSO-d_6. The smaller difference for the δ_{N-H} in **Fxo** (CDCl$_3$) compared with **Fxp/Fxm** results from the higher acidity of the amide proton and is influenced by the *ortho*-pyridine N atom. The most distinct

feature in the **Fxx** NMR spectra is the splitting of the N—H peak into a broad doublet in the **Fox** triad (**Fop**, **Fom**, **Foo**) when using aprotic solvents such as CDCl$_3$ (supplementary material, §2; Donnelly *et al.*, 2008). This splitting results from the strong through-space nuclear spin–spin couplings ($^{1h}J_{N—H\cdots F}$ = 13–15.5 Hz), caused by the formation of a strong N—H$\cdots$F interaction between the *ortho*-F atom and amide proton (Manjunatha Reddy *et al.*, 2010). The N—H resonance is present as a broad singlet in polar solvents (DMSO-d_6, supplementary material, §2) suggesting that the intramolecular N—H$\cdots$F interaction is disrupted with resulting conformational change. Previous analysis of **Mxx** (Mocilac *et al.*, 2010) suggests that highly polar solvents (with high dielectric constants) decrease the rotational barriers, facilitating ring rotation and conformational change. This is observed when the N—H$\cdots$F$_{ortho}$ interaction is disrupted in the **Fox** triad in polar solvents such as DMSO. The IR spectra for **Fxo** triads are similar with typical strong and diffused stretching bands between 3333 and 2700 cm^{-1} with prominent

peaks distinctly present in the regions 3078, 3175 and 3112 cm^{-1}.

3.3. Crystallographic data and analysis

3.3.1. General comments. The salient **Fxx** structural features are given in Tables 1 and 2 with crystallographic details listed in the supplementary material (§4). As **Fxx** has an N—H donor and an O=C and N$_{pyridine}$ acceptor, both N—H$\cdots$N and N—H$\cdots$O=C interactions are possible, although the former is favoured. The 3 × 3 **Fxx** isomer grid is augmented by two pairs of polymorphs for **Fpm** and **Fom**. In **Fpm** the **Fpm_O** polymorph exhibits N—H$\cdots$C=O intermolecular interactions as amide$\cdots$amide $C(4)$ chains (Etter, 1990), while **Fpm_N** aggregates by $_{amide}$N—H$\cdots$N$_{pyridine}$ interactions (both in $P2_1/n$, Z' = 1). In **Fom** both polymorphs **Fom_O** and **Fom_F** exhibit N—H$\cdots$O=C intermolecular hydrogen bonding but in different space groups, with different conformations and complete molecular disorder in **Fom_O**. For the remaining isomers, **Fmm** aggregates *via*
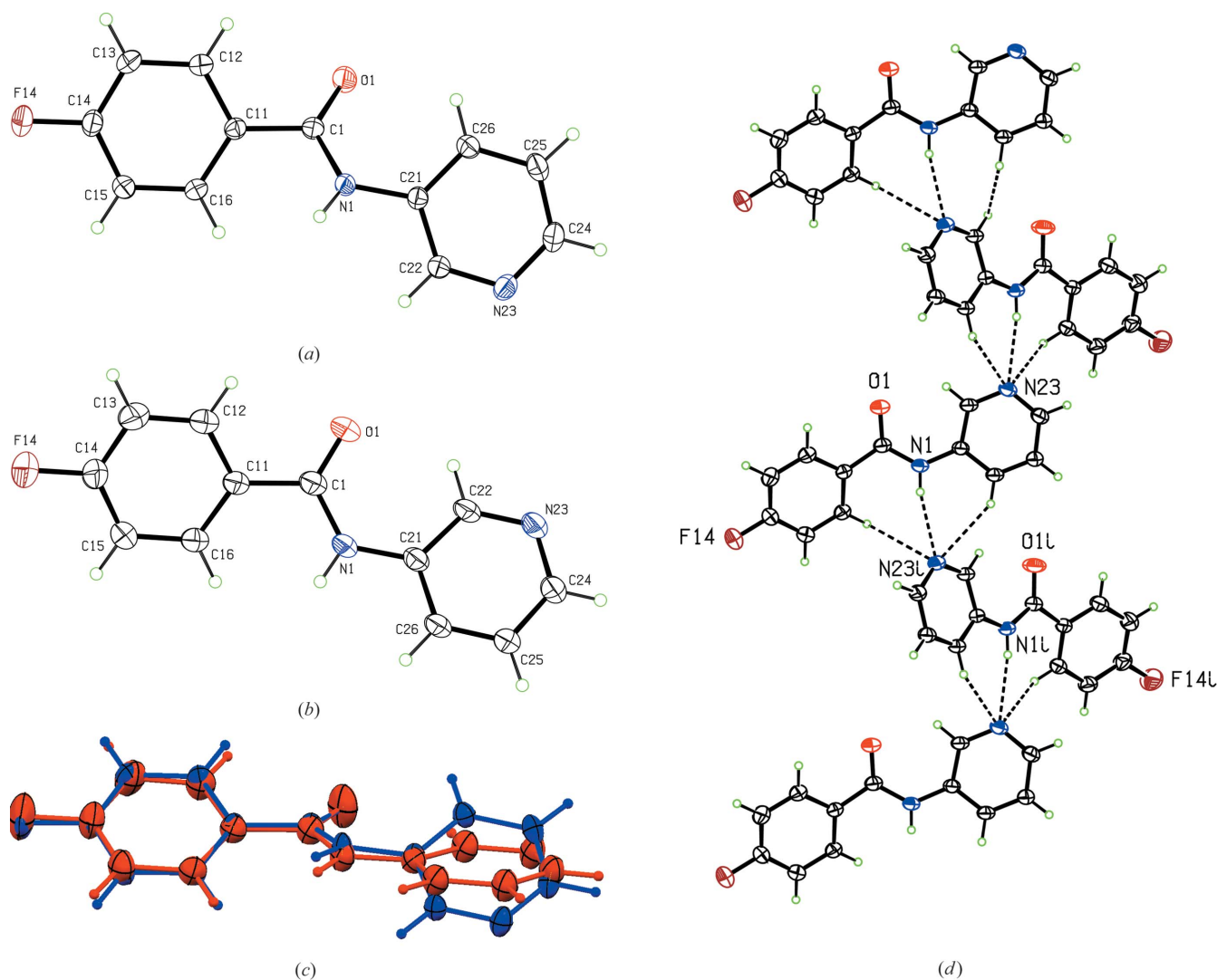
Figure 2
Views of the (*a*) **Fpm_O**; (*b*) **Fpm_N** polymorphs; (*c*) overlay of both structures with displacement ellipsoids at the 30% probability level and (*d*) a chain showing the principal and flanking N/C—H$\cdots$N$_{pyridine}$ interactions (as dashed lines) in **Fpm_N**.

Table 5
Selected structural features of the **Mxx**, **Fxx**, **NxxM** and **NxxF** isomers.

Isomer	Space group	Z/Z'	Hydrogen bonding in solid state	Conformation (solid state)	Conformation (gas phase)	Match	Amide H shift (CDCl₃, p.p.m.)
Mpp	$P2_1/n$	4/1	N—H···N	–	–	–†	8.30
Mmp	$P\bar{1}$	4/2	N—H···N	**M-syn**	**M-anti**	×	8.25
Mop	Pc	4/2	N—H···N	**M-syn|M-anti**	**M-anti**	×/√‡	8.23
Mpm	$P1$	4/4	N—H···O=C	**P-syn**	**P-syn**	√	8.11
Mmm	$P\bar{1}$	4/2	N—H···N	**M-anti/P-anti**	**M-anti/P-syn**	×	8.16
Mom	$Pca2_1$	4/1	N—H···N	**M-anti/P-anti**	**M-anti/P-syn**	×	7.98
Mpo	$P\bar{1}$	2/1	(N—H···N)₂	**P-syn**	**P-syn**	√	8.70
Mmo	$P2_1/c$	4/1	(N—H···N)₂	**M-anti/P-syn**	**M-anti/P-syn**	√	8.78
Moo	$P\bar{1}$	2/1	(N—H···N)₂	**M-syn/P-syn**	**M-anti/P-syn**	×	8.99
Fpp	$P2_1/c$	4/1	N—H···N	–	–	–†	8.01
Fmp	$P2_1/c$	4/1	N—H···N	**F-anti**	**F-anti**	√	8.01
Fop	$P2_1/c$	4/1	N—H···N	**F-syn**	**F-syn**	√	8.68
Fpm_O	$P2_1/n$	4/1	N—H···O=C	**P-syn**	**P-syn**	√	8.56
Fpm_N	$P2_1/n$	4/1	N—H···N	**P-anti**	**P-syn**	×	8.56
Fmm	$Pca2_1$	4/1	N—H···N	**F-anti/P-anti**	**F-anti/P-syn**	×	8.45
Fom_O	$P2_1$	12/6	N—H···O=C	**F-syn/P-syn|anti**	**F-syn/P-syn**	×/√§	8.53
Fom_F	$P2_1/n$	4/1	N—H···O=C	**F-syn/P-anti**	**F-syn/P-syn**	×	8.53
Fpo	$Pbcn$	8/1	(N—H···N)₂	**P-syn**	**P-syn**	√	9.04
Fmo	$P\bar{1}$	4/2	(N—H···N)₂	**F-anti/P-syn**	**F-anti/P-syn**	√	8.75
Foo	$P\bar{1}$	4/2	(N—H···N)₂	**F-syn/P-syn**	**F-syn/P-syn**	√	9.03
NppM	$P2/c$	4/1	N—H···O=C	–	–	–†	8.00
NpmM	$P2_1/n$	4/1	N—H···N	**M-anti**	**M-anti**	√	7.96
NpoM	Cc	4/1	N—H···O=C	**M-syn**	**M-syn**	√	7.90
NmpM	$P2_1/c$	4/1	(N—H···N)cat¶	**N-syn**	**N-syn**	√	8.22
NmmM	$P\bar{1}$	4/2	N—H···N	**N-anti/M-anti**	**N-syn/M-anti**	×	8.26
NmoM	$Pbca$	8/1	N—H···O=C	**N-anti/M-anti**	**N-syn/M-syn**	×	7.81
NopM	$P2_1/c$	4/1	(N—H···N)ᵢ	**N-syn**	**N-syn**	√	9.90
NomM	$P2_1$	4/2	N—H···O=C	**N-syn/M-anti**	**N-syn/M-anti**	√	9.94
NooM	$P2_1/c$	4/1	(N—H···N)ᵢ	**N-syn/M-syn**	**N-syn/M-syn**	√	10.03
NppF	$P\bar{1}$	4/2	N—H···O=C	–	–	–†	7.91
NpmF	Cc	4/1	N—H···N	**F-syn**	**F-anti**	×	8.03
NpoF	Cc	4/1	N—H···N	**F-anti** ††	**F-syn**	×	8.15
NmpF	$P\bar{1}$	8/4	(N—H···N)₄‡‡	**N-syn**	**N-syn**	√	8.44
NmmF	$P2_1/n$	4/1	N—H···N	**N-anti/F-anti**	**N-syn/F-anti**	×	8.75
NmoF	$P2_12_12_1$	4/1	N—H···N	**N-syn/F-syn**	**N-syn/F-syn**	√	8.23
NopF	$P2_1/c$	4/1	(N—H···N)ᵢ	**N-syn**	**N-syn**	√	10.04
NomF	$P2_1/n$	8/2	(N—H···N)ᵢ	**N-syn/F-anti**§§	**N-syn/F-anti**	√	10.13
NooF	$P2_1/n$	4/1	(N—H···N)ᵢ	**N-syn/F-syn**	**N-syn/F-syn**	√	10.36

† Non-applicable (n/a).   ‡ **Mop** crystallizes with two molecules in the asymmetric unit, each with different **M**-ring conformation;   § **Fom_O** polymorph has one of six molecules in the **F-syn/P-anti** conformation.   ¶ **NmpM** forms catemers.   †† Minor component only in the **F-syn** conformation.   ‡‡ **NmpF** forms tetramers.   §§ With only 3% as **F-syn**.

N—H···N interactions while all **Fxo** isomers crystallize as twisted dimers [$R_2^2(8)$ rings] via ₐₘᵢₐₑN—H···N_pyridine interactions.

3.3.2. The three isomorphous Fxp isomers. The crystal structures of the three **Fxp** compounds have been published (Donnelly *et al.*, 2008; data collected at 150 K). Nonetheless, new crystal samples were grown from ethyl acetate with data collected at 294 K in order to examine the possibility of polymorphism (Fig. 1, Tables 1–3). All three **Fxx** isomers are (as expected) isomorphous in the space group $P2_1/c$ (Donnelly *et al.*, 2008). Bond lengths and angles are normal and the C—F bond-length difference as noted previously is evident with 1.3591 (14) Å (**Fpp**), 1.3517 (16) Å (**Fmp**) and 1.3420 (15) Å (**Fop**), presumably arising from the influence of the secondary interactions/contacts and intramolecular N1—H1···F12 in (**Fop**). Of note are the structures isomorphous with the **Fxp** triad (Table 5 in McMahon *et al.*, 2008) including the parent *N*-(4-pyridyl)benzamide [MOHQOP] (Noveron *et al.*, 2002) and 2,5-difluoro-(4-pyridyl)benzamide [HOFVUU] (McMahon *et al.*, 2008). This series is unusual in that the compounds are

isomorphous (with similar unit-cell parameters, packing and alignment), but differ in their F/H peripheral atom-site position and interactions/contacts at the secondary level. This arises principally due to the *ca* 0.3–0.4 Å difference between typical organic C—F/C—H bond lengths and the resulting directional influence on weaker interactions and contacts. The **Fxp** triad is not discussed further except for comparisons (Fig. 1, Tables 1–3 and 5).

3.3.3. The Fxm isomers. *Fpm polymorphs*: The **Fpm** isomer was isolated as two polymorphs **Fpm_O** and **Fpm_N** (suffix O/N is based on the primary intermolecular interactions), both of which crystallize in the space group $P2_1/n$ with $Z' = 1$ (Brittain, 2011; Bernstein, 2011; Figs. 2a–d). The IR spectra of both polymorphs show distinct differences in the N—H stretching region (2800–3400 cm⁻¹) with **Fpm_O** having a sharp peak at 3325 cm⁻¹ and characteristic of amide···amide (N—H···O=C) hydrogen-bonded benzamides/pyridinecarboxamides, while **Fpm_N** has a diffuse pattern of N—H stretching bands indicative of N—H···N interactions. The IR spectrum of the bulk **Fpm** powder shows a diffuse peak pattern

suggesting a prevalence of the **Fpm_N** polymorph and this seems to be preferred as the **Fpm_O** polymorph was isolated by chance.

The **Fpm_O** polymorph grown from CH_2Cl_2 (Fig. 2*a*) has N—H···O=C primary hydrogen bonding as $C(4)$ chains, while **Fpm_N** (ethyl acetate) has intermolecular N—H···N interactions as $C(5)$ chains. It is rather unusual (although not unknown) that both polymorphs crystallize in $P2_1/n$ and differ primarily in their primary interactions (Gebreslasie *et al.*, 2011; Brittain, 2011). The **Fxx** series with a strong N—H donor and two O=C/pyridine N acceptors offers the possibility of obtaining at least two different structures with either or possibly even both N—H···N/N—H···O=C interactions, although in practice one type is clearly favoured for a particular **Fxx** isomer. In **Fpm_O** the N—H···O=C interaction [N1···O1^i = 3.0575 (13) Å; (i) $x, y + 1, z$] links **Fpm** molecules into one-dimensional chains along the *b*-axis direction and parallel to the (101) plane. The remaining interactions are weak with one-dimensional chains (running antiparallel) linked by C15—H15···N23 [C15···N23^{ii} = 3.5891 (17) Å, (ii) $1 - x, 1 - y, -z$] contacts into columns, with additional weak C14—F14···F14—C14^{iii} = 2.8982 (18) Å [(iii) $2 - x, -y, -z$] contacts. The pyridine **P**-ring conformation in **Fpm_O** is **P-syn** and the aromatic rings are almost parallel though with the amide group twisted from both rings (Table 2). The **Fpm_O** molecular geometry (torsion angles) differs considerably from **Fpm_N** which is typical of benzamide geometries (Table 2), however, the most significant bond length/angle difference is C1—N1—C21 = 125.76 (10) (**Fpm_O**) and 127.7 (2)° (**Fpm_N**).

Aggregation in **Fpm_N** (Fig. 2*d*) is principally by N1—H1···N23 interactions [N1···N23^i = 3.151 (3) Å, (i) $-\frac{1}{2} + x, \frac{1}{2} - y, -\frac{1}{2} + z$] forming one-dimensional *zigzag* chains along the *c*-axis direction and parallel to the ($\bar{1}$01) plane. This N—H···N interaction is augmented by flanking C16—H16···N23^i and C26—H26···N23^i interactions [C16/C26···N23^i = 3.403 (3)/3.390 (3) Å] similar to the flanking C—H···N interactions noted in **NmpF** and **NmpM** (Mocilac *et al.*, 2011; Mocilac & Gallagher, 2011). The one-dimensional chains are linked into two-dimensional sheets by weak C—H···F interactions [H24···F14^{ii} = 2.57 Å, C24···F14^{ii} = 3.107 (3) Å, (ii) $\frac{3}{2} - x, -\frac{1}{2} + y, \frac{1}{2} - z$] along the [010] direction. There are no other direction-specific interactions present.
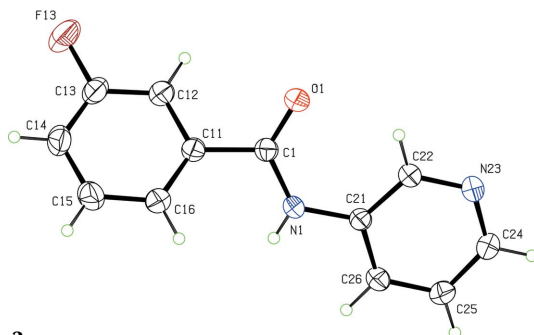
The most striking difference between **Fpm_N** and **Fpm_O** (Figs. 2*a*–*c*, Scheme 2) is the **P-anti** conformation (in **Fpm_N**) and opposite to **P-syn** in **Fpm_O** (Fig. 2*c*). This change in the pyridine ring orientation is essential for intermolecular N—H···N hydrogen bonding in **Fpm_N**. The **Fpm_O** structure resembles the related methyl derivative **Mpm** (Mocilac *et al.*, 2010). However, and in contrast to **Fpm_O**, the **Mpm** isomer crystallizes in the space group $P1$ (No. 1) with $Z' = 4$ and contains four distinct hydrogen-bonded chains formed *via* N—H···O=C interactions.

Fmm: The **Fmm** isomer (Fig. 3) shows some similarities with **Fpm_N** in terms of aggregation and conformation. As in **Fpm_N** the conformation of **Fmm** is **F-anti/P-anti** and as noted (see **Fpm** polymorphs) the **P-anti** conformation is essential for the formation of the $_{amide}$N—H···N$_{pyridine}$ hydrogen bond. The principal interaction in **Fmm** is N1—H1···N23^i [with N1···N23^i = 3.077 (3) Å, (i) $x + 1/2, 1 - y, z$] and augmented by the flanking C26—H26···N23^i [C26···N23 = 3.444 (3) Å] linking **Fmm** molecules into one-dimensional chains along the *a*-axis direction. A secondary π–π stacking interaction involves C26···C22^{ii} = 3.366 (3) Å [(ii) $-\frac{1}{2} + x, 1 - y, z$] along the *c*-axis direction and weakly connecting the one-dimensional chains into two-dimensional sheets parallel to the (010) plane. There are no other interactions of note.

***Fom* polymorphs: the unusual Fom_O with $Z' = 6$**: The **Fom** isomer was isolated as two polymorphs with **Fom_O** grown as poor quality single crystals from ethyl acetate (amongst other solvents and mixtures) after many attempts. A second polymorph, **Fom_F**, crystallized subsequently as fine, diffraction-quality single crystals by slow evaporation from methanol/diethyl ether.

The **Fom_O** polymorph crystallizes in the space group $P2_1$ ($Z' = 6$). The structure solved easily in $P2_1$ (using default settings in common structure solution programs) and even at this juncture it was obvious that **Fom_O** was disordered. On refinement the **Fom_O** structure was shown to be completely disordered with the six individual molecules having varying levels of disorder, with four molecules with a minor component (∼ 15%) and two having complete 50:50% molecular disorder. All six **Fom_O** molecules are **F-syn** as this facilitates the favourable intramolecular N—H···F$_{ortho}$ interaction as noted in the ^{1}H NMR of related benzamides (Manjunatha

Figure 3
View of the **Fmm** molecule with displacement ellipsoids at the 30% probability level.
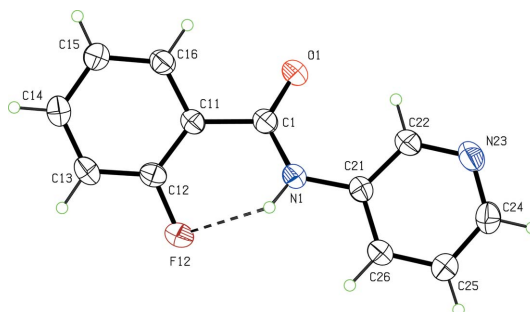
Figure 4
View of the **Fom_F** molecule with displacement ellipsoids at the 30% probability level.

Pavle Mocilac *et al.* · Structural systematics and conformational analyses

Reddy *et al.*, 2010). The N···F distances for (*A*)–(*D*) range from 2.722 (5) to 2.753 (6) Å. The *meta*-pyridine ring is mostly **P-syn** with evidence for the **P-anti** conformation in at least one of the 50:50 disordered molecules (F/H). The possibility of a second conformation of the pyridine ring in the crystal structure of **Fom_O** may be needed to effect a repeat unit on crystallization, but at the cost of an asymmetric unit with $Z' = 6$.

The primary interaction comprises six distinct N—H···O=C $C(4)$ chains involving all six molecules in the *b*-axis direction with intermolecular N···O distances ranging from 3.074 (8) to 3.117 (8) Å and C_6/C_5N interplanar angles from 4.8 (4) to 9.3 (4)° for (*A*)–(*D*). The four largely ordered molecules (*A*)–(*D*) stack in a column along the *a*-axis direction with the remaining two molecules as 50:50 disordered components (*E/G*) and (*F/H*) stacking as a column in the [100] direction sandwiched between the (*A*)–(*D*) stacks. Columns of (*A*)–(*D*), (*E/G*)/(*F/H*) are linked by weak interactions/contacts. It can be demonstrated that the *ortho*-F atom plays a major role in the **Fom_O** molecular conformation, but the assembly of the structure is perplexing. The **Fom_O** crystal structure with 100% molecular disorder can be viewed as the kinetic product of imperfect crystallization and is worthy of a more detailed analysis over a range of conditions.

Analysis of the CSD (Allen, 2002) for structures with $Z' = 6$ in space group $P2_1$ reveals 42 compounds of which bis[4-(dimethylamino)phenyl]diazene oxide [XIYZOV] (Gainsford *et al.*, 2008) is a representative planar molecule. It is described as a commensurate modulation of a $P2_1/c$ parent with $\frac{1}{3}$ of the *b*-axis, and comprising two disordered molecules with an indication of disordered components in two of the remaining azoxybenzene molecules.

The **Fom_F** polymorph (Fig. 4) is isostructural with **Fpm_O** and has similar geometry features, but the conformation as (**F-syn/P-anti**) is similar to **Fpm_N**. The primary **Fom_F** interaction is the long N—H···O = C hydrogen bond [N1···O1^i = 3.3321 (17) Å, (i) $x + 1, y, z$] linking molecules into one-dimensional $C(4)$ chains along the *a*-axis direction. Apart from the intramolecular N—H···F$_{ortho}$ interaction, the N—H···O=C is the only intermolecular interaction of consequence in **Fom_F** apart from the repulsive C16—H16···H16—C16^{ii} contact (H16···H16^{ii} = 2.33 Å) and a weak C14—H14···N23^{iii} interaction linking chains [(ii) $-1 - x, 1 - y, -z$; (iii) $\frac{1}{2} + x, \frac{1}{2} - y, \frac{1}{2} + z$]. Examination of both **Fom_O/F** highlights the difficulty that **Fom** has in forming quality crystals.

3.3.4. The Fxo isomer series: dimer formation *via* N—H···N interactions. The **Fxo** triad (Figs. 5*a*–*c*) form twisted dimers as $R_2^2(8)$ rings *via* cyclic $_{amide}$N—H···N$_{pyridine}$ interactions denoted by (N—H···N)$_2$. Dimer formation *via* the pyridine *ortho*-N atom (a mandatory **P-syn** conformation) has been analysed in the **Mxo** series (Mocilac *et al.*, 2010). In **Mxo** the central [NCNH]$_2$ moiety, hydrogen-bonded as $R_2^2(8)$ rings, is essentially planar while the **Fxo** molecules, aggregating as twisted dimers, have interplanar C_5N/C_5N or [NCNH/NCNH] angles of 39.12 (4)° [34.63 (15)°] in **Fpo**, 43.66 (7)° [30.9 (16)°], in **Fmo**, and 22.18 (5)° [21.6 (6)°] in **Foo**. In the **Fxo** triad the N—H and pyridine N are excluded from further inter-

molecular interactions and the **Fxo** structures rely on weaker C—H···O/F/π or π···π secondary intermolecular interactions.

Fpo: **Fpo** crystallizes as a hydrogen-bonded $R_2^2(8)$ dimer *via* N1—H1···N22 interactions [N1···N22^i = 3.0608 (18) Å (i) $-x, y, \frac{1}{2} - z$] but in tandem with a C16···C23^i = 3.285 (2) Å
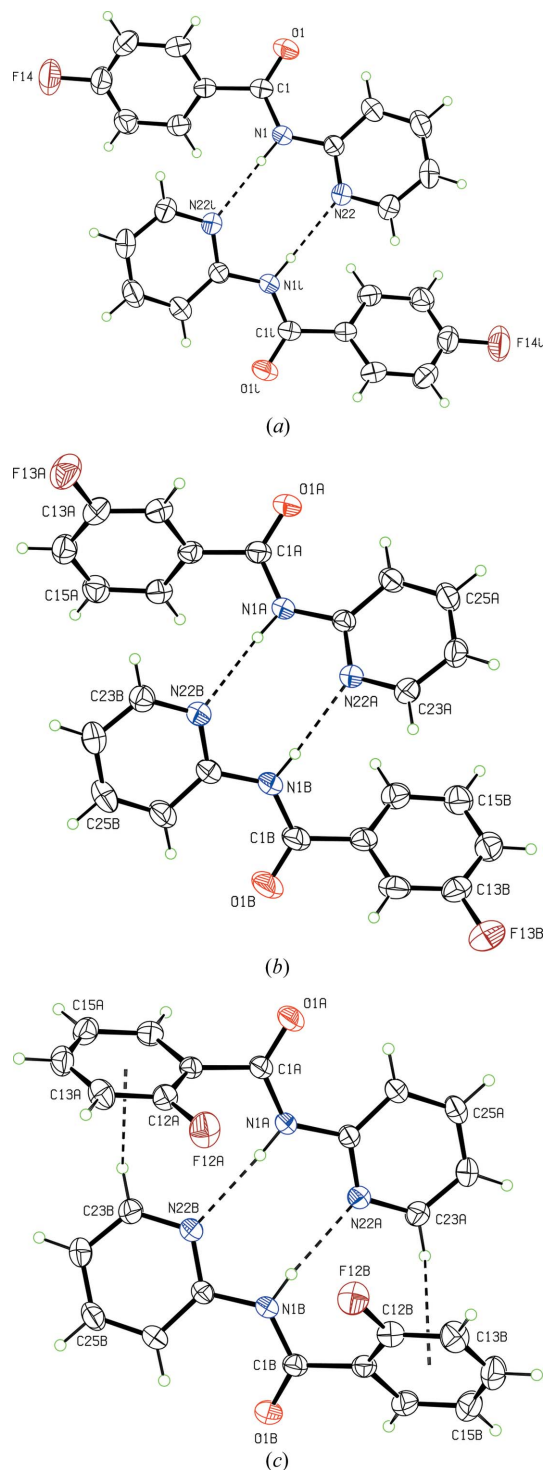
Figure 5
Views of the **Fxo** hydrogen-bonded dimers (*a*) **Fpo**, (*b*) **Fmo** and (*c*) **Foo** with displacement ellipsoids at the 30% probability level and dashed lines for the N—H···N and C—H···π interactions in **Foo**.

contact (Fig. 5*a*). Pairs of dimers are connected into tetramers by C16—H16···O1 interactions [C16···O1^{ii} = 3.266 (2) Å (ii) $x, 1 - y, \frac{1}{2} + z$] and enhanced by a C15—H15···C12 contact. Tetramers are linked into a one-dimensional column by C25—H25···O1^{iii} [(iii) $-x, y, \frac{3}{2} - z$] interactions along the *c*-axis direction. The weak C12—H12···F14^{iv} [(iv) $\frac{1}{2} + x, -\frac{1}{2} + y, \frac{1}{2} - z$] interaction alternatively interconnects one-dimensional columns into a three-dimensional structure.

***Fmo** (with the fluorine atom as a mere spectator)*: **Fmo** forms a twisted dimer through two distinct N1—H1···N22 interactions [N1A···N22B = 3.0721 (17) Å and N1B···N22A = 3.0502 (18) Å] as the **Fmo** molecules (*A/B*) are not identical (Z' = 2; Fig. 5*b*) and augmented by additional C16$_{A/B}$···C23$_{B/A}$ contacts [both contacts = 3.237 (2) Å]. Dimers are linked into tetramers by two weak C—H···O contacts [C16A—H16A···O1B^{ii}, C15B—H15B···O1A^{iii}; (ii) $1 - x, 1 - y, 1 - z$, (iii) $1 - x, 2 - y, 1 - z$] with tetramers interconnected into a one-dimensional column by stronger C25A—H25A···O1B [C25A···O1B^i = 3.235 (2) Å, (i) $x, 1 + y, z$] interactions in the *b*-axis direction. Columns are further linked into a two-dimensional sheet parallel to the [10$\bar{1}$] plane by double π···π stacking [C13A···C15A^{iv}, (iv) $-x, 1 - y, -z$] and C14B···C14B^v [(v) $2 - x, 2 - y, 2 - z$] contacts. It is unusual that the F13A/B atoms (**F-anti**) do not play significant roles in the **Fmo** crystal structure apart from indirectly influencing the offset π···π stacking contacts.

Foo: The **Foo** crystal structure assembles in a similar fashion to **Fmo** at the primary level (Z' = 2; Fig. 5*c*) and the interplanar angle between the two pyridinyl rings C_5N_A/C_5N_B) as **P-syn** is the smallest among the **Fxo** dimers.

The **Fo** rings as **F-syn** allow the formation of three contacts as N1—H1B···F12B [N1B···F12B = 2.7981 (15) Å] and C23—H23···π(C11,...,C16) with H23A···Cg1B = 2.82 Å, C23A—H23A···Cg1B = 138°, while H23B···Cg1A = 2.70 Å, C23B—H23B···Cg1A = 149°, stabilizing the dimer. In **Foo** the C23—H23$_{A/B}$···π(arene)$_{B/A}$ interactions are similar although not as significant as the analogous C—H···π(arene) interactions in **Moo** (Mocilac *et al.*, 2010; Nishio *et al.*, 2009), which has one of the shortest intermolecular C—H···π(arene) interactions described in a neutral organic system. In **Foo** the **Fo** rings (**F-syn**) with interplanar angles of 69.56 (5)° have F12A···F12B atom separations of 4.7995 (15) Å.

Dimers aggregate into tetramers by two π···π contacts with C21A···C24B^i = 3.257 (2) Å [(i) $-x, -y, 2 - z$] and C24B—H24B···π(C21A,...,C26A)^i. These are interconnected along the *b*-axis into a one-dimensional column by weak C—H···O contacts [H25B···O1A^{ii} = 2.62 Å, (ii) $x, -1 + y, z$, and C26A···O1A^{iii} = 3.225 (2) Å (iii) $-x, 1 - y, 2 - z$]. There are no other interactions of note.

3.4. Melting-point analysis: correlation with *para-/meta-/ortho*-substituent position

The design of new materials continues unabated with a preoccupancy to maximize distinct physicochemical properties, *e.g.* fluorescence, optical properties, with thermal stability and melting-point behaviour regarded as relatively unim-

portant. Even though an enormous quantity of melting point data are available in the chemical literature and from databases, the prediction of melting points of organic compounds remains difficult, although correlations of classes of organic compounds have provided some distinct trends (Brown & Brown, 2000; Slovokhotov *et al.*, 2004; Katritzky *et al.*, 2010; Preiss *et al.*, 2011).

The melting point results (Table 3) for the **Mxx**, **NxxM**, **NxxF** and **Fxx** isomer grids demonstrate that trends previously noted in disubstituted benzenes (Brown & Brown, 2000; Slovokhotov *et al.*, 2004) for *meta-* < *ortho-* < *para*-substitution show similar patterns, but with distinct combinations producing both the highest and lowest melting-point ranges. Melting-point differences of between 62 and 112 K are observed between the highest (**$**) and lowest (*) melting points in each of the four [3 × 3] grids. While melting-point behaviour depends on many factors the following trends are clear.

There is a decrease in the average melting point from the symmetrical **pp** (*para–para*) compounds to the **Fmo/Mmo** and **NomF/M** with the trend following Carnelly's rule (Brown & Brown, 2000). All four **F/Mmo**, **NomF/M** compounds possess an *ortho*-pyridine ring N atom in combination with a *meta*-F/CH$_3$ C_6 aromatic ring substituent. The four systems with **oo** substituents have higher melting points by *ca* 20 K (range from 338 to 389 K, average = 366 K) compared with the four **mo/om** derivatives (range from 333 to 352 K, average = 344 K). In both **Foo** and **Moo** the formation of hydrogen-bonded dimers by cyclic (N—H···N)$_2$ interactions is a contributory factor in their observed higher melting points (§3.3.4; Mocilac *et al.*, 2010).

Comparisons between the **Fxx** (404 K melting point average) and **Mxx** (389 K) series with **NxxF** (390 K) and **NxxM** (386 K) series demonstrate that the average melting points are remarkably similar (except for **Fxx**), although the ranges and order of melting point trends are unique within each of the four series. The average *para*-isomer has a melting point of 410 K, average *meta*-isomer is 388 K and the average *ortho* isomer 375 K (from 20 of 36 isomers containing each *p*-/*m*-/*o*-substituent). This explains why the overall melting point trend is *p* > *m* > *o*, but not the observed substitution pattern whereby the **mo/om** combinations have the lowest melting points. Comparisons of the **Fxx**, **Mxx**, **NxxM** and **NxxF** grids reveal that correlation of the melting points demonstrate the significance of the (**M/F**) substituent position on overall melting point behaviour rather than the nature of the (**M/F**) substituent. Our results suggest that in the on-going strive to maximize and tweak certain physicochemical properties that proper consideration be given to the thermal stability and behaviour of closely related aromatic isomers especially if they are combinations of di-substituted aromatics.

3.5. Ab *initio* calculations

3.5.1. Geometry optimization results. The main geometric parameters of the **Fxx** isomers optimized in the *gas phase* (using three different basis sets) for torsion angles C12—

C11—C1=O1 (α), C1—N1—C21—C26 (β) and O1—C1—N1—C21 (δ), are presented in the supplementary material (Table 3, §5) with the average difference in Table 4. Herein, torsion angles (α, β, δ) for the *gas phase* and solvated forms (CH₂Cl₂, H₂O) using the implicit solvation model PCM-SMD (Marenich *et al.*, 2009) and B3LYP/6-311++G** basis set are listed in Table 4.

In general when examining geometry, the *relative* and *absolute* benzamide geometry should be differentiated depending on whether the (*syn-*/*anti-*) conformation is neglected or endorsed. If the conformation is taken into account then the given geometrical parameter values (torsion angles) are regarded as absolute geometry. Conversely, if conformation is neglected then the relative values of the geometry are provided, in order to emphasize the relative molecular shape and for comparisons with other isomers having different conformations.

Our analysis demonstrates that the 6-311++G** basis set is optimal for **Fxx** in terms of cost. For **Fxx** the additional polarization function (6-311++G**) does not yield a significant change in the relative geometric parameters in the *gas phase* compared with the 6-311++G basis set (supplementary material). However, the polarization function influences the preferred conformation of the **Fm** ring making the **F-*anti*** slightly preferable to **F-*syn***. Alternatively, exclusion of diffuse

functions (but with added polarization functions as 6-311G**) barely alters the α dihedral (**F**-ring) angle.

A prominent feature of the modelled **Fxx** isomers is the molecular planarity in the **Fox** triad. Optimization of the **Fox** isomers suggests the presence of intramolecular N—H⋯F$_{ortho}$ hydrogen bonding between the *ortho*-fluorine and amide group (regardless of basis set) and this is responsible for the **Fox** planarity. Optimization (using the solvation model) shows that the **Fox** triad are relatively planar in low polar solvents (CH₂Cl₂, CDCl₃), while in highly polar solvents (H₂O, DMSO) the N—H⋯F$_{ortho}$ interaction distorts from planarity (**Fom**/**Foo**: α = −7.14 ± 0.73°; β = −4.22 ± 0.36°; δ = −0.26 ± 0.60°). The hypotheses (from calculations) are seen in ¹H NMR (CDCl₃; DMSO) with the N—H⋯F$_{ortho}$ interaction and **Fox** triad planarity existing in low polarity solvents, but this can be perturbed in more polar solvents (§3.2).

The remaining **Fpx**/**Fmx** isomers optimized in the *gas phase* have relatively uniform geometries with the **F**-ring rotated (α = −23.68 ± 1.40°), **P**-ring slightly rotated (β = −4.48 ± 1.06°) and with a planar amide dihedral angle (δ = −2.66 ± 0.28°). The **Fpx**/**Fmx** isomers optimized in CH₂Cl₂ agree (α = −25.01 ± 0.52°; β = −5.92 ± 1.64°; δ = −2.58 ± 0.42°), but in H₂O the **F**-ring and amide dihedral angle are similar for the *gas phase* and CH₂Cl₂ (α = −24.88 ± 0.88°, δ = −2.83 ± 0.79°), however, the **P**-ring differs. In **Fpp**, **Fpm** and **Fmm** the **P**-ring
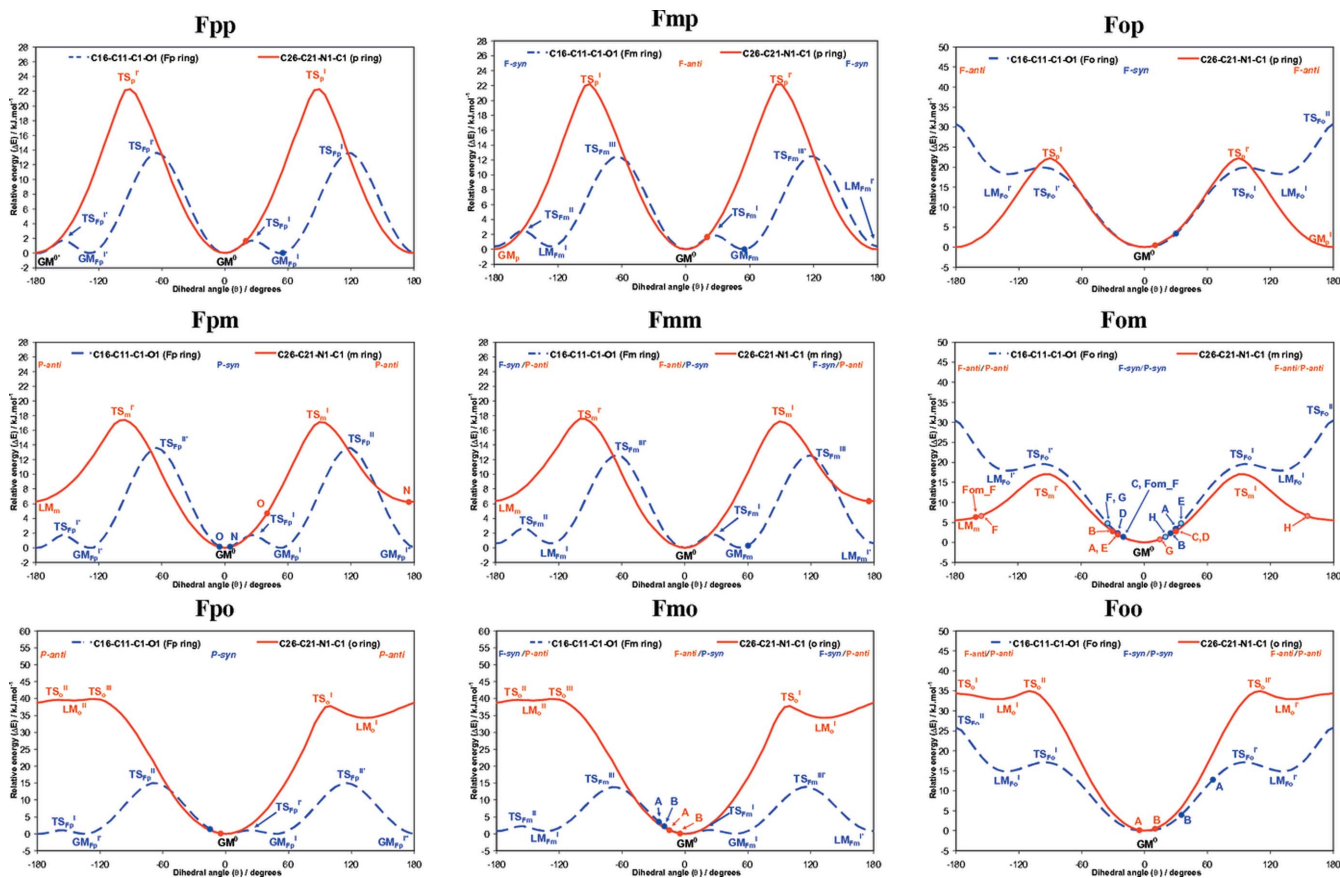
Figure 6
The **Fxx** PES conformational analyses optimized in the *gas phase*: the equivalent solid-state angle is depicted as a filled circle, with, if applicable, assigned identification letter and/or polymorph designation.

exhibits increased rotation ($\beta = -13.68 \pm 2.38°$), while for **Fmp**, **Fpo** and **Fmo** it is similar to CH_2Cl_2 ($\beta = -6.15 \pm 0.55°$). A similar increase in twist angle and influenced by a high dielectric field was noted for the **Mxx**, **NxxF** and **NxxM** isomers (Mocilac *et al.*, 2010, 2011; Mocilac & Gallagher, 2011).

3.5.2. Conformational analysis. The nine PES conformational analysis diagrams of the **Fxx** isomers (*gas phase*, 6-311++G** basis set) are depicted in Fig. 6. Detailed descriptions of the PES profiles with high-resolution diagrams are provided (supplementary material, §5.3). The **F-ring** (α dihedral angle) is shown as a **blue dashed line**, whereas the **P-ring** (β dihedral angle) is a **full red line**. At $\theta = 0$ and $\pm180°$, the conformation of the asymmetric F- or P-ring is described as *syn* or *anti*. Conformational analyses without the polarization (**/d,p) or diffuse (++) functions (supplementary material, diagrams 5.5, 5.7 and 5.8) generally give analogous PES diagrams with main rotational barrier and energy increases at unstable conformational states.

The **Fxx** and **Mxx** isomer grids are congeneric derivatives of the same *N*-pyridinylbenzamide template (Scheme 1). Comparisons of the **Fxx** and **Mxx** PES diagrams (Mocilac *et al.*, 2010) reveal a high degree of similarity, especially for the **Fpx** and **Fmx** triads. As expected and due to the modelled **Fox** triad planarity, the **Fo** rings in the **Fox** isomers have symmetrical PES profiles and different to the **Mo** ring (**Mxx**), but similar to the **oF** ring PES profiles in **NxoF** (Mocilac *et al.*, 2011). As for related isomer grids (Mocilac *et al.*, 2010, 2011; Mocilac & Gallagher, 2011) the modularity of the **Fxx** isomers allows a systematic approach in the analysis and classification of the PES profiles depending on substituent position (*para-*/*meta-*/*ortho-*), and for comparisons with **Mxx** (Mocilac *et al.*, 2010).

The asymmetric **Fxx** isomers (having at least one non-*para* ring) exhibit a preference for the **F-syn/P-syn** conformation except for **Fmx** where the **F-anti** conformation is found to be slightly more stable. The *para*-fluorophenyl (**Fp**) ring gives a PES profile with two global and two local maxima, with four equivalent global minima. The *meta*-fluorophenyl (**Fm**) ring has two global and two local maxima, but two global (**F-anti** conformation) and two local minima (**F-syn** conformation). As expected, the difference between the two conformations is small (~ 0.6 kJ mol^{-1}) and from Boltzmann distribution at ambient temperatures, *ca* 56% of molecules have the thermodynamically preferred **F-syn** conformation. In reality, a kinetic equilibrium between the **F-syn/F-anti** conformation exists (Mocilac *et al.*, 2010).

In §3.5.1 the **Fox** triad optimization gives planar models (regardless of the basis set) and predicts a six-membered ring formed *via* the $N-H\cdots F_{ortho}$ interaction. In **NooF** a similar five-membered ring, with a symmetrical **oF** ring PES profile has been noted (Mocilac *et al.*, 2011). In comparison to **NooF**, it was expected that the six-membered ring in **Fox** with a better oriented donor/acceptor would provide stronger hydrogen bonding. However, a comparison of the **Fo** and **oF** PES diagrams (using the 6-311++G basis set) shows that TS_{oF}^{I} in **NooF** and TS_{Fo}^{I} in **Fox** are equal (~ 25.25 kJ mol^{-1})

suggesting a similar $N-H\cdots F_{ortho}$ interaction strength in both systems.

Conformational analyses of the pyridinyl rings show similar results to the **Mxx** grid (Mocilac *et al.*, 2010). The *para*-pyridinyl ring (**p**) has two equal global minima, while the *meta*-pyridinyl ring (**m**) has one global minimum (**P-syn** conformation) and one local minimum (**P-anti** conformation) with a difference of ~ 6 kJ mol^{-1} between the two conformers. The conformer preference is not altered by excluding the polarization or diffuse functions from the basis set (6-311++G**) (supplementary material, diagram 5.7). The *ortho*-pyridinyl ring (**o**) gives a PES profile with one strong global minimum (**P-syn** conformation) and unstable high-energy regions from ±90 to $\pm180°$.

The main feature of the **Fx** ring PES in different solvents compared with the *gas phase* is the uneven difference in the decrease/increase of rotational barriers and local minima throughout the **Fxx** series, as noted in **Mxx** (Mocilac *et al.*, 2010). In the PES of solvated **Fx** rings, the isomers can be divided into three main groups: **Fpp/m**, **Fmp/m**, **Fox**, while in **Fpo** and **Fmo** the influence of solvation is more pronounced. However, it is seen that the influence of solvents is relatively minor in the **Fp** and **Fm** rings (especially in **Fpp/m** and **Fmp/m**), while in **Fo** a strong decrease is noted.

In **Fpp/m**, where the solvation model influence is small, the main rotational barrier TS_{Fp}^{II} decreases by $\sim 9\%$ in CH_2Cl_2 ($\sim 7\%$ in H_2O). In contrast the TS_{Fp}^{I} increases by $\sim 14\%$ in CH_2Cl_2 (decrease of $\sim 7\%$ in H_2O). This phenomenon noted in **Mxx** can be explained partially by the fact that the TS_{Fp}^{I} has molecules in a planar conformation and a higher dielectric field can destabilize this conformation.

The PES behaviour of the **Fm** ring in the **Fmp/m** isomers is slightly different to **Fp** with a similar small drop in the main rotational barrier TS_{Fm}^{III}. Regardless, there is a significant decrease of LM_{Fm} and TS_{Fm}^{II} that effectively matches the **F-syn** and **F-anti** conformations and especially in a high dielectric solvent: the **F-syn/F-anti** difference for all **Fmx** isomers solvated in CH_2Cl_2 is small at 0.38 kJ mol^{-1} (0.16 kJ mol^{-1} in H_2O). In **Fpo** and **Fmo** a decrease at TS_{Fm}^{III} is more pronounced ($\sim 16\%$) as well as the increase at $TS_{Fm}^{I/II}$ ($\sim 36\%$ in CH_2Cl_2, $\sim 65\%$ in H_2O).

For the **Fo** ring the behaviour in solvents is even for all three **Fox** isomers with a strong decrease of the rotational barriers. These results reflect the influence of the dielectric field in the hindrance of intramolecular interactions (as $N-H\cdots F_{ortho}$), whereas spectroscopic data (supplementary material, §2) demonstrate hydrogen-bond disruption in polar solvents (^{1}H NMR in DMSO-d_6 versus CDCl$_3$, supplementary material).

Conformational analyses of the pyridinyl rings with the solvation model show significant decreases of the rotational barriers and local minima in both solvents. For the *para*-pyridinyl ring (**p**) the rotational barrier TS_p decreases by 8% in CH_2Cl_2 (18% in H_2O), while for the *meta*-pyridinyl ring (**m**) the decrease of the TS_m rotational barrier is 25% (45%). The significant finding is that the LM_m decreases by 60% in CH_2Cl_2 (80% in H_2O). According to Boltzmann distribution it signifies (at ambient temperature in polar solvents such as

water, DMSO or methanol) that $\sim 38\%$ of **Fxm** molecules are expected to have their **m** rings as **P-anti**, while in less polar solvents (CH$_2$Cl$_2$, EtOAc) $\sim 25\%$ of **Fxm** molecules are **P-anti**. Finally, the rotational barriers of the *ortho*-pyridine rings (**o**) evenly decrease by $\sim 40\%$ in CH$_2$Cl$_2$ and $\sim 63\%$ in H$_2$O.

4. Comparison of experimental and calculated Fxx structures

Comparison of the **Fxx** structures from crystal structure data and calculations is shown by difference marks (●), marking the torsion angle differences ($\Delta\theta$) between the experimental and theoretical structures on the corresponding *gas phase* PES diagram curves (Fig. 6). For structures with $Z' > 1$ (as **Fom_O**, **Fmo**, **Foo**), data from each molecule is labelled with corresponding capitals. The data for particular polymorphs are labelled as **O**, **N** (**Fpm**) and **Fom_F**. In the case of the **Fom_O** polymorph only the angles of the main components are assigned labels.

In general most crystal structure conformations and dihedral angles correlate well with their modelled versions (Mocilac *et al.*, 2010, 2011; Mocilac & Gallagher, 2011) and especially for the **Fxp** and **Fxo** isomers where the average deviation from the nearest global minimum (GM) is only 11–24° for both rings.

The **Fxp** isomers are isomorphous and their solid-state geometries are almost identical with minor differences (Donnelly *et al.*, 2008; see §3.3.2, Fig. 1). However, while the **Fpp** and **Fmp** have the difference labels (●) on similar positions close to the global minima, in **Fop** the dots (●) are shifted as the modelled **Fop** structure is supposed to be planar, and different from both **Fpp** and **Fmp**. In the solid state **Fop** adopts a similar geometry to **Fpp** and **Fmp**, and partially retains the intramolecular N1—H1···F12 interaction. The **F**-ring rotation from planarity is necessary in order to facilitate N1—H1···N24 hydrogen bonding. In contrast, **Fpp** and **Fmp** at their global minima (GM^0) are in an almost ideal position for intermolecular hydrogen bonding and crystal structure formation. Crystal growth of the **Fxp** triad is relatively easy in most organic solvents and their high melting point ranges reflect the stability and strength of the **Fxp** crystal structures. Their physical behaviour might be influenced by similarities between the geometry of the optimized models and solid state structures.

The **Fxm** triad (comprising the polymorphs) reveals some interesting features (§3.3.3). One key element is the frequent occurrence of the *meta*-stable **P-anti** conformation (in **Fpm_N**, **Fmm** and **Fom**). This result is in accordance with the structures (**Mom**, **Mmm**, **NmmF** and **NmmM**) that have their *meta*-pyridine rings in a **N/P-anti** conformation (Mocilac *et al.*, 2010, 2011; Mocilac & Gallagher, 2011). It is clear that the **P-anti** conformation is favourable for the formation of intermolecular N—H···N hydrogen bonds as it positions the pyridine N atom and the amide N—H with opposite orientations suitable for molecular aggregation *via* N—H···N *zigzag* chains.

Fpm_O has the same **P-syn** conformation as the optimized structure with the **P**-ring slightly rotated towards co-planarity with the **Fp** ring (Fig. 2a). The stable **P-syn** conformation arranges molecules in the correct conformation for N—H···O=C hydrogen-bond formation and co-planar rings can form additional contacts between the one-dimensional chains. The more common **Fpm_N** polymorph as **P-anti** is suitable for N—H···N interactions (Fig. 2b). Of note is that the energy levels of the **P**-rings are similar for both polymorphs while their **F**-rings are located at the global minimum (GM).

As expected from previous studies (Mocilac *et al.*, 2010, 2011; Mocilac & Gallagher, 2011) and similar to **Fpm_N** (Fig. 2b), **Fmm** is **F-anti**/**P-anti** (Fig. 3) and almost strictly residing in global/local minima without significant deviation from the stationary points. The same conformation is present in all *meta*-ring '**N/Xmm(X)**' derivatives. Therefore, both *meta*-pyridinyl and *meta*-substituted phenyl rings (regardless of the nature of substituents) prefer the ***anti*** conformation in combination with intermolecular N—H···N primary interactions.

A study of **Fpm** (Figs. 2a–d) and 4-fluoro(N-4-halo-3-pyridyl)benzamides has demonstrated the versatility of the benzamide scaffold in drug discovery and structure activity relationship (SAR) studies with **Fpm** studied as a K$_v$7 (KCNQ) modulator (ztz252) (Gao *et al.*, 2010). Using calculations (Fig. 6) it would be of interest to examine and compare the actual binding mode (conformational preference) of **Fpm** in a K$_v$7 (KCNQ) channel (Ashcroft, 2006).

The **Fom** isomer, isolated as the completely disordered **Fom_O** and ordered **Fom_F** (Fig. 4) has the **Fom_F** conformation **F-syn**/**P-anti**, while for **Fom_O** one molecule (F/H) of six exhibits the **F-syn**/**P-anti** mode with the remaining **Fom_O** as **F-syn**/**P-syn**. The structures of both **Fom** polymorphs are relatively planar with rings rotated by ± 15–35° and this partially complies with modelling results as **Fom** is predicted to be planar both in the *gas phase* and solvents (Table 4, §3.5.1). **Fom_F** has essentially the same shape as **Fpm_N**, but with the conformation and space group as for **Fpm_O**. However, with the F$_{ortho}$, an additional intramolecular N—H···F$_{ortho}$ interaction forms and hinders any conformation other than **F-syn**, and influences the observed disorder in **Fom_O** (with mostly **P-syn**) and preventing the same supposed structural organization as in **Fpm_O** (**P-syn**). Having the **P**-ring in the **P-anti** arrangement disrupts the intramolecular N—H···F$_{ortho}$ interaction. The main factors influencing polymorph formation experimentally are solvent and crystallization rate. The **Fom_F** polymorph crystallizes from CH$_3$OH by slow evaporation. From the modelling analysis, solvents with higher polarity can facilitate the necessary conformational changes (from **P-syn** $\rightarrow$ **P-anti**), while slower evaporation is often known to produce better quality crystal growth. The **Fom_O** polymorph crystallizes from a less polar solvent (EtOAc) under faster crystallization conditions. Therefore, it seems that under these conditions the **Fom** molecules cannot fully adopt the favourable **P-anti** conformation, but rather aggregate (where possible) with a high level of disorder. Nevertheless, a comparison of both polymorphs

gives the impression that the **Fom_O** polymorph is, in fact, an imperfect variant of **Fom_F**.

In the **Fxo** triad (Fig. 5), all crystal structure conformations correspond closely with the calculated models with similar dihedral angles and small but moderate distortions from the global minima (5 → 25°). The only major difference is in **Foo** where the **Fo** rings are rotated by 65° (molecule *A*) and 35° (molecule *B*). This twist is primarily due to steric reasons as the formation of the hydrogen-bonded $R_2^2(8)$ rings does not allow the **Fo** ring to adopt a planar geometry. The intramolecular N1—H1*B*···F12*B* interaction decreases the dihedral angle in molecule *B*, while in molecule *A* increased rotation allows the formation of favourable C—H···π interactions. This trade-off between N—H···F/C—H···π(arene) interactions does not arise in **Moo** as dimer formation by cyclic N—H···N interactions is exclusively augmented by very short C—H···π(arene) interactions with H···Cg = 2.46 Å [2.33 Å normalized] (Mocilac *et al.*, 2010; Nishio *et al.*, 2009).

5. Comparisons of the Mxx, Fxx, NxxM and NxxF isomer grids

The salient features of all 36 **Mxx**, **Fxx**, **NxxM** and **NxxF** benzamide/pyridinecarboxamide isomers and two additional polymorphs are listed in Table 5. This details the crystallographic and solid-state results (space group, *Z*/*Z'*, primary interaction, solid-state conformation), modelling data (*gas phase* conformation) and ^{1}H NMR (amide N—H shift, CDCl$_3$) with melting-point trends (§3.4). Although benzamides and pyridinecarboxamides are not, strictly speaking, congeneric, they have, sharing similar moieties, a high level of similarity (apart from the reversed amide bridge) that facilitates comparisons.

The primary hydrogen bonding in the crystal structures of all 38 structures can be analysed in four groups. The most common interaction is the $_{amide}$N—H···N$_{pyridine}$ *zigzag* chain in 18 structures. This usually arises in molecules where the pyridine N atom is positioned *para* or *meta* and while having N *para* makes the N—H···N convenient, isomers with *meta*-N usually have to have their **P** or **N** rings in a *meta*-stable *anti* conformation. This is the case with all '**XmmX**' compounds and the **Fpm_N** polymorph. Exceptions include the tetrameric **NmpF**, catemeric **NmpM**, mixed methyl/fluoro system **NmpFM** (Mocilac & Gallagher, 2011) and **NmoF** (Mocilac *et al.*, 2011). A second group of nine structures has the less common N—H···O=C hydrogen bonding as *C*(4) chains and is present in some **NxxF/M** isomers such as **NppF**, **NppM**, **NpoM** and **NmoM**. The **Mpm** isomer and **Fpm_O** aggregate by N—H···O=C interactions with similar structures, as well as **Fom_O** (*P-syn*) and **Fom_F** (*P-anti*). The **NomM** structure forms N—H···O=C hydrogen bonds unexpectedly, however, the presence of an intramolecular (N—H···N)$_i$ interaction hampers the stability of N—H···O=C hydrogen bond and **NomM** has a low melting point (323 K), where there was considerable difficulty in growing diffraction quality crystals (Mocilac & Gallagher, 2011).

The third group comprises the six **Mxo** and **Fxo** isomers where the pyridine N atom is positioned *ortho* and therefore plays a unique role in dimer formation. Two N—H···N interactions form a $R_2^2(8)$ ring (Etter, 1990) by the perfect match of **Mxo** molecular pairs but less so for **Fxo**. This arrangement is labelled as (N—H···N)$_2$ in Table 5 and is similar to the (*R*COOH)$_2$ carboxylic acid dimers seen in centrosymmetric carboxylic acids. The **Mxo** and **Fxo** solid-state and modelled conformations almost always match, except for **Moo** where the **Mo** ring rotates in order to accomplish the important and short C—H···π(arene) interaction (Mocilac *et al.*, 2010; Nishio *et al.*, 2009). The *ortho*-N thus causes an additional acidity in the amide hydrogen as noted in the ^{1}H NMR and seen as a small additional deshielding effect (Table 5). The fourth group comprises the **NoxM** and **NoxF** isomers. Here the pyridine nitrogen is positioned *ortho*- but due to the amide linkage reversal, the amide hydrogen is now directed towards the pyridine N atom facilitating the formation of intramolecular N—H···N interactions designated by (N—H···N)$_i$. The weakening of the amide hydrogen is seen in further deshielding in the ^{1}H NMR (CDCl$_3$). In **NooF** the N—H···F$_{ortho}$ interaction additionally deshields the amide hydrogen ensuring its chemical shift is the lowest for all compounds (at 10.36 p.p.m.).

There is a distinct lack of variation in the N···O/N distances (Å) in both the **Fxx** and **Mxx** isomer grids and the range is rather narrow at *ca* 0.11 Å (apart from **Fom_F**). For the **Fxo** triad twisted dimers form *via* cyclic $_{pyridine}$N—H···N$_{amide}$ interactions as $R_2^2(8)$ rings and are distinctly different to the **Mxo** triad. This highlights the subtle differences and effects of the F atoms and methyl groups that are peripheral to the primary cyclic N—H···N interactions. The **Fxx** analyses highlight the predominance of N—H···N interactions as the primary hydrogen bonding in comparison to amide···amide (as N—H···O=C). The **Fxx** results correlate well with **Mxx**, but contrast with **NxxF/NxxM** where the predominance of the N—H···N interactions drops to 2:1.

The hydrogen-bonding type is also discerned using IR spectroscopy. The presence of the N—H···N interaction gives a diffuse pattern of weak peaks from 3400 to 2800 cm^{-1}, whereas N—H···O=C hydrogen bonding is detected by a sharp peak at *ca* 3300 cm^{-1}. The cyclic (N—H···N)$_2$ hydrogen bonding has an intricate set of elevated and merged medium peaks ranging from 3180 to 2900 cm^{-1} and all isomers with (N—H···N)$_i$ hydrogen bonding have a very strong and sharp peak *ca* 3330 cm^{-1}. Of note in the unusual **NomM** isomer (Mocilac & Gallagher, 2011) where both N—H···O=C and (N—H···N)$_i$ hydrogen bonding occurs is that the relevant N—H and C=O stretching vibrations are shifted to lower wavenumbers than would have been anticipated (N—H at 3286 cm^{-1}).

Our study of the four **Fxx**, **Mxx**, **NxxM** and **NxxF** isomer grids has facilitated an indepth analysis of the solid-state and computational models for 36 compounds in 2 × 18 isomer sets as well as being able to investigate correlations when examining physicochemical trends, *e.g.* melting points (Mocilac *et al.*, 2010, 2011; Mocilac & Gallagher, 2011). Of particular

interest is that in *ca* 35% of cases the solid state and computationally derived structures (global minima, GM^0) do not coincide. This is of relevance especially in the modelling of more complex molecules in guest:host systems (Brameld *et al.*, 2008) where the models and diffraction derived data may differ due to local minima (LM)/saddle points being mistaken/mis-identified for global minima (GM^0), a phenomenon frequently encountered in the chemical literature. This theme will be examined and developed by us in future research.

6. Conclusions

Crystal structure analyses of the **Fxx** isomer grid shows that eight form N—H···N hydrogen bonds and only one isomer (**Fom**) aggregates *via* intermolecular N—H···O=C interactions, exclusively. For the **Fxo** triad, twisted dimers form as cyclic $R_2^2(8)$ rings *via* N—H···N interactions in contrast to the hydrogen-bonded chains in the **Fxp** and **Fxo** triads. Moreover, both **Fpm** and **Fom** crystallize with two polymorphs. Computational modelling and conformational preferences of the **Fxx** grid demonstrate that the solid-state conformations generally conform with the most stable calculated conformations except for the **Fxm** triad. Calculations involving the **Fox** triad predict the intramolecular N—H···F$_{ortho}$ interaction, as established both by spectroscopic and crystallographic data.

Of particular note is that *ca* 35% of the molecules studied in our $4 \times [3 \times 3]$ isomer grids have different conformations in the solid state and *ab initio* geometry optimizations in a three torsion angle system (reduced to two with the amide (δ) considered invariant due to multiple bond character). This disparity varies little with basis set and the incorporation of additional diffuse/polarization functions. Analysis using solvation models show a decrease in the rotational barriers with increasing polarity, facilitating interconversion between distinct conformations/rotamers. While solid-state computational calculations will enable more comparisons and provide more answers in future research, the important message is that the use of solid-state (crystallographic) experimental results for *ab initio* geometry optimizations may only optimize to a local minimum (LM) and not the global minimum (GM^0). Calculations at local minima are only valid for the particular local minimum and not a complete representation of the conformational preferences. It is critically important to analyse (scan) all relevant torsion angles ($\pm 180°$) where possible and rank preferences in order of importance so as to get a 'true' picture of the conformational preferences. The importance of the Cambridge Structural Database for comparisons and in facilitating both conformational preferences and torsion angle ranking should also be considered (Allen & Motherwell, 2002; Brameld *et al.*, 2008; Cruz-Cabeza & Allen, 2012).

In our 3×3 isomer grid, **Fmm** is an example where the solid-state and calculated results do not match. In related series the **Mmm** and **Mom** (Mocilac *et al.*, 2010), **NpmF**, **NpoF** and **NmmF** (Mocilac *et al.*, 2011), **NmmM** and **NmoM** (Mocilac & Gallagher, 2011) amongst others, it has been demonstrated that the computational and experimental results

do not coincide. Comparisons of the **Fxx** isomer grid with the **Mxx**, **NxxM** and **NxxF** isomer series (**M** = methyl) reveal a high degree of similarity in solid-state aggregation and physicochemical properties, while correlation of the melting point data indicates the significance of the (**M/F**) substituent position on melting point behaviour rather than the nature of the (**M/F**) substituent.

References

Allen, F. H. (2002). *Acta Cryst.* B**58**, 380–388.
Allen, F. H. & Motherwell, W. D. S. (2002). *Acta Cryst.* B**58**, 407–422.
Ashcroft, F. M. (2006). *Nature*, **440**, 440–447.
Berger, R., Resnati, G., Metrangolo, P., Weber, E. & Hulliger, J. (2011). *Chem. Soc. Rev.* **40**, 3496–3508.
Bernstein, J. (2011). *Cryst. Growth Des.* **11**, 632–650.
Brameld, K. A., Kuhn, B., Reuter, D. C. & Stahl, M. (2008). *J. Chem. Inf. Model.* **48**, 1–24.
Brittain, H. G. (2011). *J. Pharm. Sci.* **100**, 1260–1279.
Brown, R. J. C. & Brown, R. F. C. (2000). *J. Chem. Educ.* **76**, 724–731.
Chopra, D. & Row, T. N. G. (2008). *CrystEngComm*, **10**, 54–67.
Chopra, D. & Row, T. N. G. (2011). *CrystEngComm*, **13**, 2175–2186.
Cruz-Cabeza, A. J. & Allen, F. H. (2012). *Acta Cryst.* B**68**, 182–188.
Donnelly, K., Gallagher, J. F. & Lough, A. J. (2008). *Acta Cryst.* C**64**, o335–o340.
Etter, M. C. (1990). *Acc. Chem. Res.* **23**, 120–126.
Frisch, M. J. *et al.* (2010). *GAUSSIAN*09, Revision B. 01. Gaussian Inc., Wallingford, CT, USA.
Gainsford, G. J., Bhuiyan, M. D. H. & Kay, A. J. (2008). *Acta Cryst.* E**64**, o874–o875.
Gallagher, J. F., Donnelly, K. & Lough, A. J. (2009a). *Acta Cryst.* E**65**, o102–o103.
Gallagher, J. F., Donnelly, K. & Lough, A. J. (2009b). *Acta Cryst.* E**65**, o486–o487.
Gao, Z., Zhang, T., Wu, M., Xiong, Q., Sun, H., Zhang, Y., Zu, L., Wang, W. & Li, M. (2010). *J. Biol. Chem.* **285**, 28322–28332.
Gebreslasie, H. G., Jacobsen, Ø. & Görbitz, C. H. (2011). *Acta Cryst.* C**67**, o283–o287.
Gelbrich, T., Hursthouse, M. B. & Threlfall, T. L. (2007). *Acta Cryst.* B**63**, 621–632.
Katritzky, A. R., Kuanar, M., Slavov, S., Hall, C. D., Karelson, M., Kahn, I. & Dobchev, D. A. (2010). *Chem. Rev.* **110**, 5714–5789.
Lu, S.-Y., Hong, J. & Pike, V. W. (2003). *J. Labelled Compd. Radiopharm.* **46**, 1249–1259.
Luthe, G., Swenson, D. C. & Robertson, L. W. (2007). *Acta Cryst.* B**63**, 319–327.
Macrae, C. F., Bruno, I. J., Chisholm, J. A., Edgington, P. R., McCabe, P., Pidcock, E., Rodriguez-Monge, L., Taylor, R., van de Streek, J. & Wood, P. A. (2008). *J. Appl. Cryst.* **41**, 466–470.

Manjunatha Reddy, G. N., Vasantha Kumar, M. V., Guru Row, T. N. & Suryaprakash, N. (2010). *Phys. Chem. Chem. Phys.* **12**, 13232–13237.

Marenich, A. V., Cramer, C. J. & Truhlar, D. G. (2009). *J. Phys. Chem. B*, **113**, 6378–6396.

McArdle, P. (1995). *J. Appl. Cryst.* **28**, 65.

McMahon, J., Anderson, F. P., Gallagher, J. F. & Lough, A. J. (2008). *Acta Cryst.* C**64**, o493–o497.

Metrangolo, P., Murray, J. S., Pilati, T., Politzer, P., Resnati, G. & Terraneo, G. (2011). *CrystEngComm*, **13**, 6593–6596.

Mocilac, P. & Gallagher, J. F. (2011). *CrystEngComm*, **13**, 5354–5366.

Mocilac, P., Lough, A. J. & Gallagher, J. F. (2011). *CrystEngComm*, **13**, 1899–1909.

Mocilac, P., Tallon, M., Lough, A. J. & Gallagher, J. F. (2010). *CrystEngComm*, **12**, 3080–3090.

Montgomery, J. A., Ochterski, J. W. & Petersson, G. A. (1994). *J. Chem. Phys.* **101**, 5900–5909.

Nishio, M., Umezawa, Y., Honda, K., Tsuboyama, S. & Suezawa, H. (2009). *CrystEngComm*, **11**, 1757–1788.

Noveron, J. C., Lah, M. S., Del Sesto, R. E., Arif, A. M., Miller, J. S. & Stang, P. J. (2002). *J. Am. Chem. Soc.* **124**, 6613–6625.

Oxford Diffraction Ltd (2010). *ABSFAC* and *CrysAlisPro CCD/RED*, Version 1. 171.33.55. Oxford Diffraction Ltd, Abingdon, Oxfordshire, UK.

Preiss, U. P., Beichel, W., Erle, A. M., Paulechka, Y. U. & Krossing, I. (2011). *ChemPhysChem*, **12**, 2959–2972.

Ren, C. L., Xu, S. Y., Xu, J., Chen, H. Y. & Zeng, H. Q. (2011). *Org. Lett.* **13**, 3840–3843.

Sheldrick, G. M. (2008). *Acta Cryst.* A**64**, 112–122.

Slovokhotov, Y. L., Neretin, A. S. & Howard, J. A. K. (2004). *New J. Chem.* **28**, 967–979.

Spek, A. L. (2009). *Acta Cryst.* D**65**, 148–155.

Wardell, S. M. S. V., de Souza, M. V. N., Vasconcelos, T. R. A., Ferreira, M. L., Wardell, J. L., Low, J. N. & Glidewell, C. (2008). *Acta Cryst.* B**64**, 84–100.

Wardell, S. M. S. V., de Souza, M. V. N., Wardell, J. L., Low, J. N. & Glidewell, C. (2007). *Acta Cryst.* B**63**, 879–895.